Biosensors and Bioelectronics 51 (2014) 76–81

Contents lists available at ScienceDirect

Biosensors and Bioelectronics

journal homepage: www.elsevier.com/locate/bios

Preparation of graphene nanoplatelet–titanate nanotube composite and its advantages over the two single components as biosensor immobilization materials

Xiaoqiang Liu [a,*], Jiamei Zhang [a], Rui Yan [a], Qingyou Zhang [a], Xiuhua Liu [b,*]

[a] Institute of Environmental and Analytical Sciences, College of Chemistry and Chemical Engineering, Henan University, Kaifeng, Henan Province, 475004, PR China
[b] Key Laboratory of Natural Products and Immunology, Kaifeng, Henan Province, 475004, PR China

ARTICLE INFO

Article history:
Received 22 June 2013
Accepted 13 July 2013
Available online 26 July 2013

Keywords:
Nanocomposite
Graphene nanoplatelets
Titanate nanotubes
Direct electron transfer
Biosensor

ABSTRACT

A novel nanocomposite consisting of graphene nanoplatelets (GNPs) and titanate nanotubes (TNTs) have been synthesized successfully utilizing the hydrothermal method. The GNP–TNT composite was characterized by transmission electron microscopy, X-ray diffraction, Fourier transform infrared spectroscopy and electrochemical impedance spectroscopy. The voltammetric characterization of GNP–TNT composite, pure GNPs and pure TNTs modified horseradish peroxidase (HRP) biosensors were conducted to select the most suitable electrode immobilization material for enzyme biosensors. The GNPs was firstly eliminated owing to its extremely high background charging current, distinct electrochemical interference from its surface functional groups and low signal to noise ratio. Next, the direct electron transfer of HRP on electrode and the catalytic current of HRP towards H_2O_2 was increased around 45% and 72% respectively on GNP–TNT composite modified electrodes compared with those on pure TNTs modified electrodes. GNP–TNT composite modified HRP biosensor also exhibited superiority over pure TNTs modified HRP biosensor in the analytical performance. The precision and stability study provided additional evidence for the feasibility of using GNP–TNT composite as electrode modification material.

1. Introduction

In recent years, graphene-semiconductor composites especially graphene–TiO_2 composites have attracted a great deal of research interest in photocatalysis, nanoelectronics and photovoltaic devices due to their high remarkable mechanical, electrical, thermal and optical properties (Perera et al., 2012; Zhang et al., 2011). More specifically, graphene possesses excellent electronic conductivity, strong chemical inertness and high surface area (Zhang et al., 2011); TiO_2 nanomaterials have shown some features like good biocompatibility, anti-oxidizing properties, chemical inertness, high specific surface area and photocatalytic capability (Liu et al., 2012; Perera et al., 2012). Owing to the above advantages, both graphene and TiO_2 nanomaterials have been applied in the development of electrochemical biosensors individually as the key immobilization materials and direct electron transfer of redox enzymes has been achieved on both nanomaterials modified electrodes (Liu et al., 2012; Shan et al., 2009).

However, it is surprising that graphene–TiO_2 composites have rarely been used in the electrochemical biosensors hitherto. Therefore, a horseradish peroxidase (HRP) electrochemical biosensor was developed to evaluate the feasibility of using graphene–TiO_2 composites as electrode materials in this work. Herein, a few improvements have been made to minimize the disadvantages associated with the existing graphene–TiO_2 composites before applying them in the electrochemical biosensors. As graphene consists of only a single layer of sp^2-hybridized carbon atoms, graphene sheet is easily subjected to the fracture during the synthesis process of composites. In addition, graphene also suffered from poor stability resulting from its 2D-thin layer structure and the preparation method (Shao et al., 2010). As a consequence, graphene nanoplatelets (GNPs) replaced graphene to integrate with TiO_2 nanomaterials in this paper. The physical and chemical characteristics of GNPs is similar to those of graphene except that the former is thicker (more than 10 layers) and more stable than the later (Shao et al., 2010). At the same time, titanate nanotubes (TNTs) instead of TiO_2 nanoparticles were used to combine with GNPs because TNTs have higher specific surface area and can provide better interfacial contact with GNPs than TiO_2 nanoparticles (Perera et al., 2012). As an immobilization matrix, high specific surface area and excellent biocompatibility of TNTs also aid in increasing the load of redox enzymes and sustaining their bioactivity (Liu et al., 2012).

* Corresponding authors. Tel.: +86 13781157777.
E-mail addresses: xq_liu1975@yahoo.com (X. Liu), liuxiuhua@henu.edu.cn (X. Liu).

0956-5663/$ - see front matter © 2013 Elsevier B.V. All rights reserved.
http://dx.doi.org/10.1016/j.bios.2013.07.029

In the present work, a novel GNP–TNT composite was synthesized and characterized by transmission electron microscopy, X-ray diffraction and Fourier transform infrared spectroscopy. Then, room temperature ionic liquid (RTIL) and Nafion were used as binder to immobilize GNP–TNT composite and HRP onto the electrode surface to construct a biosensor. The electrochemical behavior of as-prepared biosensor was compared with TNTs/RTIL/Nafion/HRP biosensor and GNPs/RTIL/Nafion/HRP biosensor using cyclic voltammetry. The analytical performance, precision and stability of the GNPs–TNTs/RTIL/Nafion/HRP biosensor were also studied by chronoamperometry.

2. Experimental

2.1. Reagents and instruments

GNPs were purchased from Chengdu Organic Chemicals Co., Ltd., Chinese Academy of Sciences, China. Layer of GNPs is less than 30 layers and the thickness is between 4–20 nm. TiO_2 nanoparticles (P25) were bought from Tianjin Chemical Reagent Co. Ltd., China. Horseradish peroxidase and the other chemicals were purchased from Sigma-Aldrich. Electrochemical measurements were performed using a CHI630C electrochemical workstation (CH Instruments, Shanghai, China) with a conventional three-electrode system, which was constituted with a glassy carbon (GC) electrode as working electrode, a platinum wire as counter electrode and a Ag|AgCl (3.0 KCl) as reference electrode. All electrodes were purchased from Gaoshiruilian Co. Ltd., Wuhan, China. Electrochemical impedance spectroscopy was carried out using an IM6ex electrochemical station (ZAHNER, Germany). The morphological characterization and chemical composition of the composite was investigated by field emission transmission electron microscopy (FETEM, Tecnai G2 20, FEI Co. Ltd., USA), X-ray diffraction (XRD, X-PertPro, Netherland) with Cu Kα radiation (λ=1.5406 nm), and Fourier transform infrared spectra (FT-IR, Nicolet 170, USA).

2.2. Preparation of GNP–TNT composite

The synthesis of GNP–TNT composite is described as below: 25 mg GNPs was added to 1 mL (1 mol/L) sodium dodecyl sulfate (SDS) solution. Subsequently, 19 mL deionized water was added and then the mixture was treated with ultrasonic for 1 h. After ultrasonic processing, 0.5 g P25 was added to the GNP dispersion under modest magnetical stirring. Then 20 mL (20 mol/L) NaOH aqueous solution was added and the mixture was transferred to a Teflon-lined autoclave, followed by hydrothermal reaction at 120 °C for 18 h. After hydrothermal reaction, the resulting crude product with gray color was washed with water 3 times, then adjusted with 0.1 mol/L HCl to pH 7, washed with water 3 times again, followed by centrifugation and finally grinded to powder after dried in oven at 80 °C for 5 h. The pure TNTs were prepared by a similar process without adding GNPs.

2.3. Preparation of the HRP electrode

The preparation of the HRP electrode is described briefly as below: firstly, a glass carbon electrode (GCE) with a diameter of 3 mm was polished on a polishing cloth with 0.3 mm alumina powder and washed with deionized water and ethanol successively. The polished electrode, covered with a beaker, was then dried at room temperature. The mixture of GNP–TNT, RTIL and Nafion was kept shaking at 2 °C for 4 h in a full temperature oscillation incubator before being applied on the electrode surface. Specifically, 300 μl HRP aqueous solution (2 mg/ml) and 50 μl Nafion were well mixed with RTIL and GNP–TNT composite (1:5, w/w). Finally, 4 μL of the suspension was casted on the GC electrode surface, and dried in refrigerator at 4 °C. The compared electrodes were fabricated based on the similar procedure.

2.4. Electrochemical measurements

During the process of electrochemical measurements, the working solutions were deoxygenated with nitrogen gas for 15 min firstly and then a nitrogen atmosphere was kept over the solutions until the test was over. In amperometry, a constant potential of −0.4 V was applied to the working electrode, then hydrogen peroxide and hydroquinone were injected into the electrochemical cell after the baseline current has stabilized and the response current was recorded. EIS was conducted in the presence of 5.0 mmolL^{-1} $K_3[Fe(CN)_6]$ and 0.1 molL^{-1} KCl via applying an AC voltage with 4 mV amplitude in a frequency range from 100 kHz to 1 mHz under open circuit potential conditions and plotted in the form of Nyquist plots.

3. Results and discussion

3.1. FT-IR, XRD, TEM and EIS characterization of nanomaterials

The FT-IR spectra of pure TNTs (trace a), pure GNPs (trace b), and GNPs–TNTs (trace c) are shown in Fig. 1(A). The broad absorption from 3000 to 3700 cm^{-1} in all three traces are attributed to the O–H stretching vibration of surface hydroxyl from adsorbed water (Zhang et al., 2009). In trace a, the low frequency absorption below 1000 cm^{-1} is assigned to the Ti–O–Ti vibration (Neumann et al., 2005). While in trace c, the absorption band corresponding to Ti–O–Ti vibration (below 1000 cm^{-1}) becomes wider compared with that in curve *a*. In the previous report, this absorption band is attributed to the combination of Ti–O–Ti and Ti–O–C vibration, indicating that the chemical bonds were built between GNPs and TNTs (Iwabuchi et al., 2004). The FT-IR spectrum of graphene nanoplatelet (trace b) showed the typical skeletal vibration adsorption band of C=C at about 1638 cm^{-1}, C–OH at about 1387 cm^{-1}, C=O stretching band at about 1742 cm^{-1} and C–O stretches at about 1073 cm^{-1} (Feng et al., 2012; Tung et al., 2011), demonstrating the abundant existence of the oxygen-containing functional groups on its surface. After the formation of GNP–TNT nanocomposite (trace c), the characteristic adsorption bands of oxygen-containing functional groups at about 1742 cm^{-1} and 1073 cm^{-1} (trace b) disappeared, indicating that the amount of the oxygen-containing functional groups in GNP–TNT nanocomposite was reduced significantly.

The XRD patterns of TNTs, GNPs and GNPs–TNTs are displayed as Fig. 1(B) trace a, b and c respectively. As shown in trace a and c, the characteristic diffraction peaks at around 9.6° is assigned to the tubular structure of TiO_2 nanomaterials, indicating that TNTs have been produced successfully (Zhang et al., 2004). In addition, the diffraction peaks at 2θ angles of about 25.4°, 37.6°, 48.1°, 54.1°and 62.8° can be indexed to the (101), (004), (200), (105), (211) and (204) crystal faces of phase-pure anatase TiO_2 nanomaterials (Pizem et al., 2002). In trace b, the large peak at 2θ angles of 26° is attributed to the high crystallinity (002) of GNPs (Xu et al., 2010). However, this typical diffraction peak of GNPs decreased dramatically in the XRD pattern of GNP–TNT composite as displayed in trace c, which may be due to its overlap with the (101) peak of anatase TiO_2.

TEM images of GNPs and GNPs–TNTs shown in Fig. 2 (A) provide powerful evidence that TNTs have grown on the surface of GNPs using P25 as precursor. Fig. 2(A)(a) is the TEM image of GNPs and we can see that GNPs are semitransparent

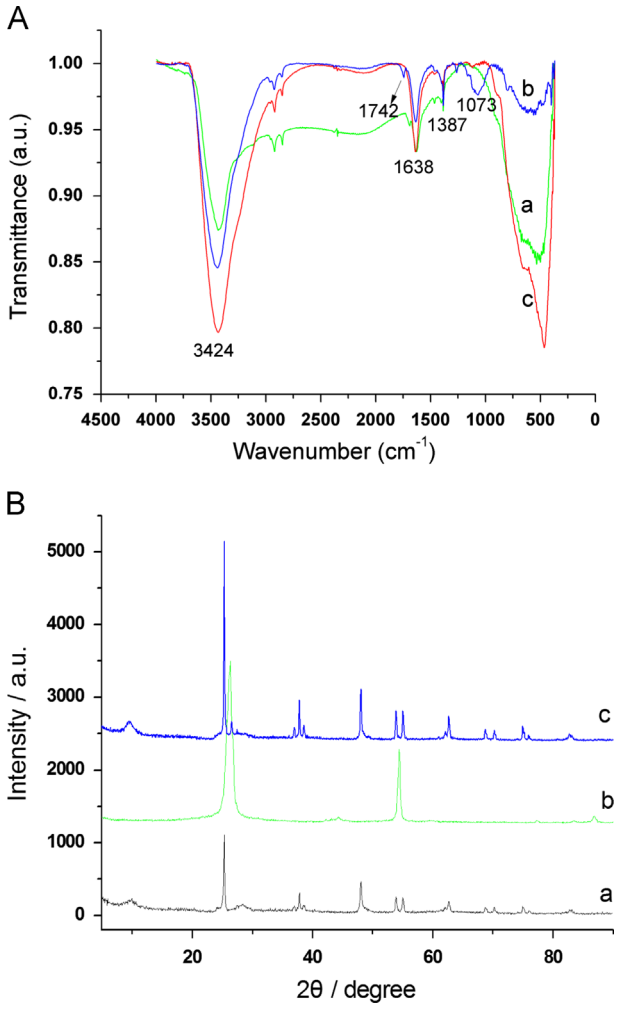

Fig. 1. (A) FT-IR spectra of (a) TNTs, (b) GNPs, and (c) GNPs–TNTs; (B) XRD pattern of (a) TNTs, (b) GNPs, and (c) GNPs–TNTs.

sheet with large surface area (about few micrometers in the diameter) which is an advantage for growing TNTs on their surface. As displayed in Fig. 2(A)(b), TNTs have been loaded on the wrinkled GNP surface using the hydrothermal method. In addition, the bundles and clusters of TNTs have occupied most of the GNP surface except the edge, demonstrating a high load of TNTs in the composite. From an enlarged TEM image of GNP–TNT composite (Fig. 2(A)(c)), the average diameter of TNTs was estimated to be about 10 nm.

Electrochemical impedance spectroscopy (EIS) was conducted to evaluate the electrical conductivity of the three electrode materials: GNP–TNT nanocomposite, GNPs and TNTs. In EIS, the semicircle diameter of the Nyquist plot of $-Z''$ against Z' at high frequency region represents the interface electron-transfer resistance (R_{et}); while the linear section at low frequency region corresponds to the diffusion control process. We can see from Fig. 2(B) that the GNPs modified electrode exhibited almost a straight line (curve *a*), indicating a nearly complete diffusion control process and an excellent electrical conductivity. While after being bonded with TNTs, the R_{et} of GNP–TNT nanocomposite (curve *b*) increased slightly compared with that of GNPs, giving evidence of slightly lower electrical conductivity in comparison with pure GNPs. It is estimated from curve *c* that the R_{et} of TNTs is approximately 700 Ω, demonstrating a relatively large interface electron-transfer impedance of TNTs. Therefore, the sequence of electrical conductivity for three electrode materials is GNPs > GNP–TNT nanocomposite > TNTs.

3.2. Electrochemical characterization of the HRP electrode

HRP biosensors using GNP–TNT composite, pure GNPs and pure TNTs as electrode immobilization materials have been constructed respectively. The electrochemical behaviors of these biosensors were compared by cyclic voltammetry to determine which one is the most appropriate electrode material for the development of biosensors. Fig. 3(A) shows the cyclic voltammograms of GNPs/RTIL/Nafion /GCE with the absence (trace a) and presence (trace b) of HRP in the composite film. Although direct electron transfer of HRP has been achieved on GNPs modified electrodes, both electrodes exhibited extremely large charging currents. At the same time, a small couple of redox peaks appeared on GNPs/RTIL/Nafion/GCE, which is probably attributed to the electrochemical interference from the oxygen-containing functional groups on GNPs surface. All of above disadvantages associated with GNPs will deteriorate sensitivity and signal-noise ratio of the GNPs modified biosensors, therefore GNPs alone is not an appropriate electrode material for enzyme biosensors. Next, the electrocatalytic performance of HRP in both GNPs–TNTs and TNTs modified electrodes were studied to make a selection between these two electrode immobilization materials. Cyclic voltammograms of TNTs/RTIL/Nafion/GCE (trace a) and TNTs/RTIL/Nafion/HRP/GCE in the absence (trace b) and presence (trace c) of 1.0 mmolL^{-1} H_2O_2 are shown in Fig. 3(B). While, Fig. 3(C) displayed the cyclic voltammograms of GNPs–TNTs/RTIL/Nafion/GCE (trace a) and GNPs–TNTs/RTIL/Nafion/HRP/GCE without (trace b) and with the presence (trace c) of 1.0 mmolL^{-1} H_2O_2. In these cyclic voltammetric experiments, same amount of GNPs–TNTs and TNTs were applied on the electrode surface and the quantity of HRP on all the modified electrodes is also equal. In the absence of H_2O_2, the redox current of HRP on the GNPs–TNTs modified electrodes (Fig. 3(C), trace b) has increased about 45% compared with that of the TNTs modified electrodes (Fig. 3(B), trace b), indicating that direct electron transfer of HRP on electrode was facilitated in the GNPs–TNTs matrix. It is also observed that the catalytic reduction current of the GNPs–TNTs/RTIL/Nafion/HRP/GCE (Fig. 3(C), trace c) towards H_2O_2 has enhanced about 72% compared to that of the TNTs/RTIL/Nafion/HRP/GCE (Fig. 3(B), trace c), demonstrating a better catalytic effect of HRP in the GNP–TNT matrix than that in the TNT matrix. As calculated from Fig. 3, the charging current difference is less than 6% between TNT/RTIL/Nafion/GCE (Fig. 3(B), trace a) and GNPs–TNT/RTIL/Nafion/GCE (Fig. 3(C), trace a), therefore the enlarged electrochemical signal of GNP–TNT modified biosensor is mainly attributed to the improved electrical conductivity and biocompatibility of the nanocomposite instead of electrode surface area.

3.3. Analytical applications of the HRP biosensor

Fig. 4(A) shows the cyclic voltammograms of (a) GNPs–TNTs/RTIL/Nafion/HRP/GCE and (b) TNTs/RTIL/Nafion/HRP/GCE in the presence of 0.1 mmolL^{-1} hydroquinone and 1.0 mmolL^{-1} H_2O_2. Herein, hydroquinone was used as an electron mediator to facilitate electron transfer of redox enzyme on electrode and to enhance electrochemical signal for the purpose of quantitative determination. As can be seen from Fig. 4(A), hydroquinone can improve the sensitivity of the biosensors significantly because the reduction currents of both biosensors were increased 625% and 692% respectively compared with those in the absence of hydroquinone (Fig. 3 (C) trace c and Fig. 3(B) trace c). The catalytic reduction peaks for both biosensors reached maximum values when applied potentials were lower than −0.25 V. Therefore, a potential of −0.4 V was applied in the following chronoamperometric experiments to guarantee the full catalytic reduction of H_2O_2. The catalytic currents of GNPs–TNTs/RTIL/Nafion/HRP/GCE is

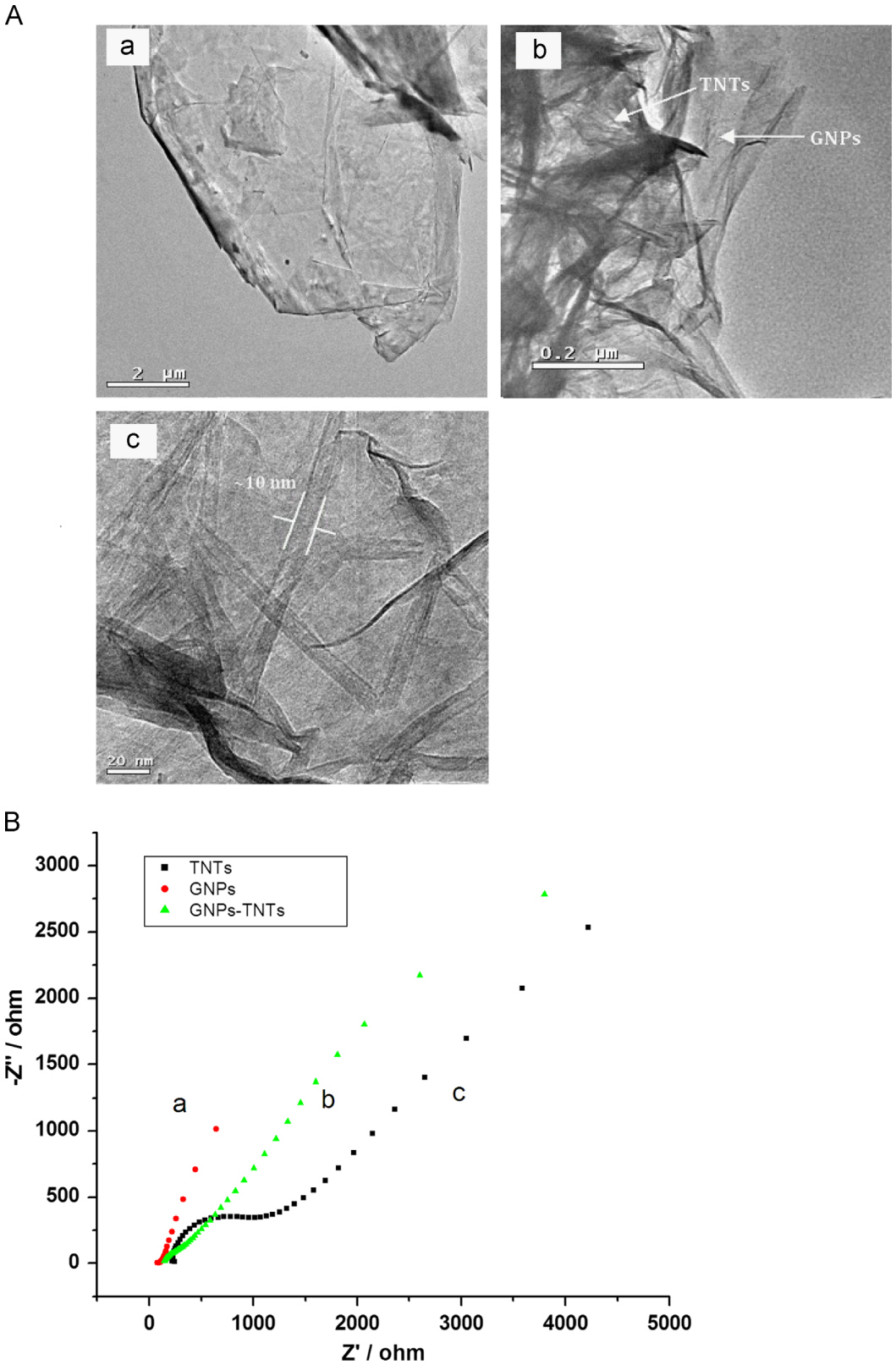

Fig. 2. (A) TEM images of (a) GNPs, (b) GNP–TNT composite at 0.2 μm scale and (c) GNP–TNT composite at 20 nm scale; (B) Nyquist plots of (a) GNPs/GCE, (b) GNPs–TNTs/GCE and (c) TNTs/GCE in a solution of 5.0 mmolL^{-1} $K_3[Fe(CN)_6]$ and 0.1 molL^{-1} KCl with the frequencies ranging from 100 kHz to 1 mHz.

67.2% larger than that of TNTs/RTIL/Nafion/HRP/GCE, indicating the advantages of GNP–TNT nanocomposite over pure TNTs as electrode materials.

The analytical performance of TNTs/RTIL/Nafion/HRP/GCE and GNPs–TNTs/RTIL/Nafion/HRP/GCE was evaluated using chronoamperometry. The droplets of 50 μL H_2O_2 (35 mmolL^{-1}) was added

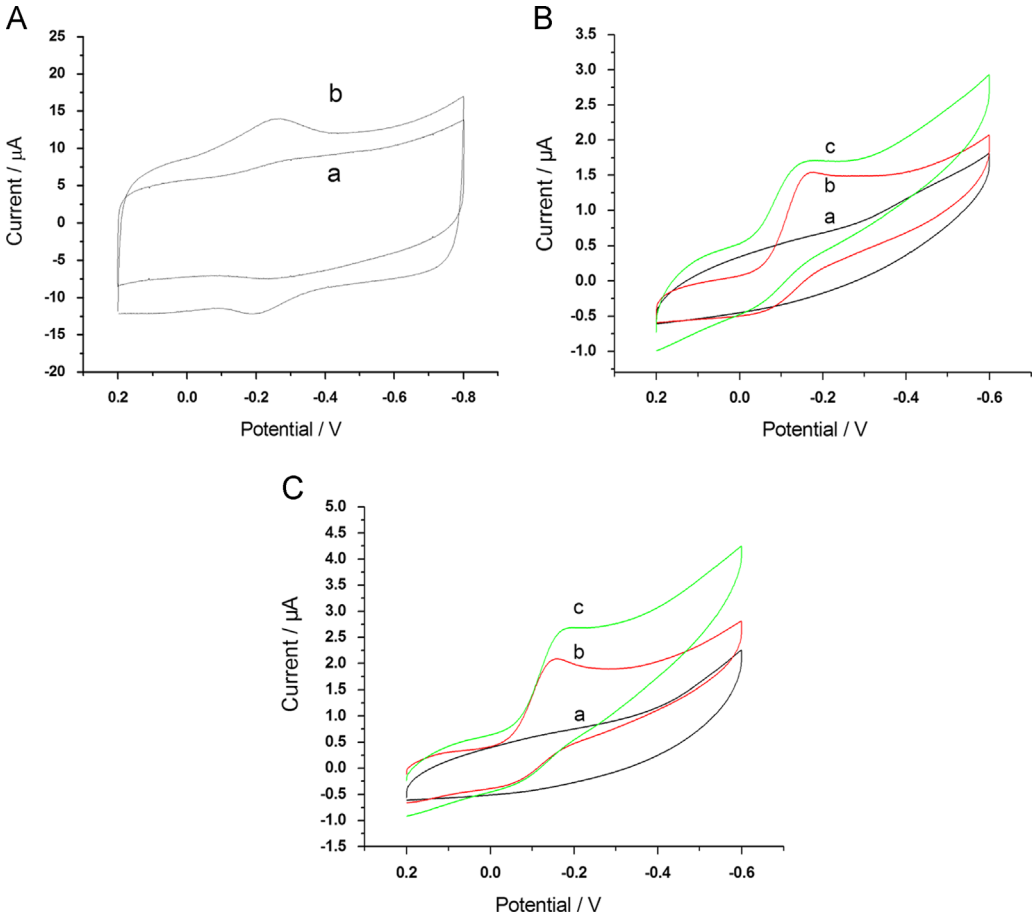

Fig. 3. (A) Cyclic voltammograms of GNPs/RTIL/Nafion composite film (trace a) and GNPs/RTIL/Nafion/HRP composite film-modified GC electrodes (trace b) in 50 mmolL^{-1} PBS (pH=7.0) with N_2-saturated at a scan rate of 50 mVs^{-1}; (B) cyclic voltammograms obtained at TNTs/RTIL/Nafion/GCE (trace a), TNTs/RTIL/Nafion/HRP/GCE in the absence (trace b) and presence (trace c) of 1.0 mmolL^{-1} H_2O_2 in 50 m molL^{-1} N_2-saturated PBS (pH=7.0) at a scan rate of 50 mVs^{-1}; and (C) cyclic voltammograms obtained at GNPs–TNTs/RTIL/Nafion GCE (trace a), GNPs–TNTs/RTIL/Nafion/HRP/GCE in the absence (trace b) and presence (trace c) of 1.0 mmolL^{-1} H_2O_2 in 50 mmolL^{-1} N_2-saturated PBS (pH=7.0) at a scan rate of 50 mVs^{-1}.

into 30 mL PBS (50 mmolL^{-1}, pH=7.0) under moderate stirring successively to make a final concentration of 58.3 μmolL^{-1} H_2O_2 in 30 mL PBS for each addition. Amperometry was conducted by applying a constant potential of −0.4 V in the presence of 0.1 mmolL^{-1} hydroquinone. As Fig. 4(B) represents, the amperometric response at both biosensors increased stepwise with successive additions of H_2O_2. However, the current at GNPs–TNTs/RTIL/Nafion/HRP/GCE (trace a) is obviously bigger than that at TNTs/RTIL/Nafion/HRP/GCE (trace b) in the presence of the same H_2O_2 concentration. The inset in Fig. 4(B) shows the calibration plots constructed based on the current versus time plots in Fig. 4(B). For GNPs–TNTs/RTIL/Nafion/HRP/GCE (trace a), the calibration plot between 58.3 and 991.1 μmolL^{-1} can be represented by the following linear relationship (with a statistical significant correlation coefficient of 0.993 at the 95% confidence level):

$$\text{Peak current}/\mu A = (8.20 \pm 0.235) \times 10^{-3}/\mu A\ \mu M^{-1}\ [H_2O_2] + (3.73 \pm 0.127)$$

The corresponding calibration plot obtained for TNTs/RTIL/Nafion/HRP/GCE (trace b) can be expressed as (with a statistical significant correlation coefficient of 0.996 at the 95% confidence level):

$$\text{Peak current}/\mu A = (4.35 \pm 0.306) \times 10^{-3}/\mu A\ \mu M^{-1}\ [H_2O_2] + (4.11 \pm 0.137)$$

From the two linear relationships above, we figured out that the sensitivity of the former HRP biosensor is 88.5% bigger than that of the later one, which could be contributed to the better electrical conductivity and biocompatibility of GNPs–TNTs nanocomposite than those of pure TNTs.

3.4. Precision and stability study of the GNPs–TNTs/RTIL/Nafion/HRP/GCE, TNTs/RTIL/Nafion/HRP/GCE and GNPs/RTIL/Nafion/HRP/GCE

Precision and stability studies were conducted to further assess the performance of all three biosensors. Precision study normally includes two tests: one is reproducibility (intra-assay) and the other is repeatability (inter-assay). Reproducibility test was studied based on results obtained with 6 HRP biosensors fabricated in a single batch in 0.5 mmolL^{-1} H_2O_2 and a relative standard deviation of 7.5% was achieved; and for repeatability test, a relative standard deviation of 8.9% was obtained after 8 successive measurements at a concentration of 0.5 mmol L^{-1} H_2O_2. While, the precision of TNTs/RTIL/Nafion/HRP/GCE is 8.2% for reproducibility test and 9.3% for repeatability test respectively, which are slightly inferior to those of GNPs–TNTs biosensor. The stability test was conducted by measuring the average amperometric responses of 6 biosensors after 1 day, 3 days, 1 week and 2 weeks and the results were compared to those obtained on the first day. As shown in Table 1, an average drop of 5.5% in the amperometric response after 3 days, 13% after 1 week and 19% after 2 weeks on GNPs–TNTs modified HRP biosensor, which is

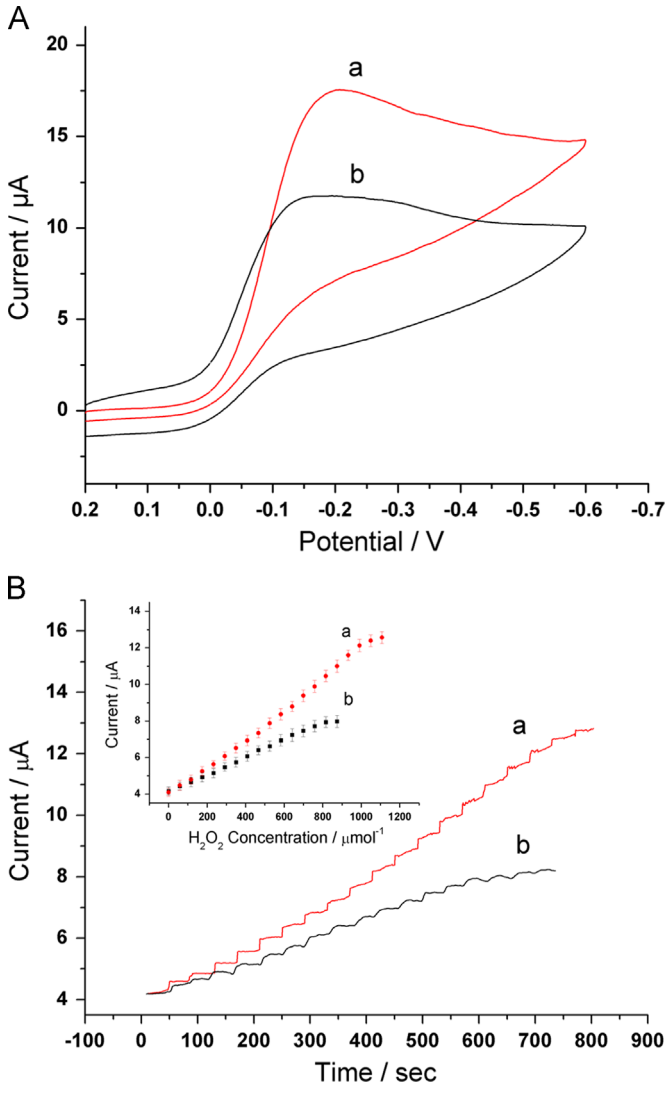

Fig. 4. (A) Cyclic voltammograms of (a) GNPs–TNTs/RTIL/Nafion/HRP/GCE and (b) TNTs/RTIL/Nafion/HRP/GCE in the presence of 0.1 mmolL^{-1} hydroquinone and 1.0 mmolL^{-1} H_2O_2 in 50 mmolL^{-1} PBS (pH=7.0); (B) chronoamperometry response of (a) GNPs–TNTs/RTIL/Nafion/HRP/GCE and (b) TNTs/RTIL/Nafion/HRP/GCE in the presence of 0.1 mmolL^{-1} hydroquinone with additions of H_2O_2 (final concentration of 58.3 μmolL^{-1} in 30 mL PBS solution for each addition) in 50 mmolL^{-1} PBS (pH=7.0) at the operating potential of −0.4 V. Inset: relationship between the catalytic current and the concentration of H_2O_2, (a) GNPs–TNTs/RTIL/Nafion/HRP/GCE and (b) TNTs/RTIL/Nafion/HRP/GCE.

Table 1
The amperometric response drop of GNPs–TNTs, TNTs and GNPs modified HRP biosensors to H_2O_2 after 3 days, 1 week and 2 weeks.

HRP sensors evaluated in this work	3 days	1 week	2 weeks
GNPs–TNTs modified HRP sensor (%)	5.5	13	19
GNPs modified HRP sensor (%)	8.4	18.5	34
TNTs modified HRP sensor (%)	6.2	14.8	21.5

preferable to pure GNPs, pure TNTs modified HRP biosensors and the other relevant published sensors (Gao et al., 2013; Xiao et al., 2011). All above results demonstrated the feasibility of using GNPs–TNTs as electrode immobilization material in the construction of HRP biosensors.

4. Conclusions

The GNP–TNT composite has been synthesized and characterized through TEM, XRD, FT-IR and EIS. The electrical conductivity of the GNP–TNT nanocomposite was confirmed to be superior to that of pure TNTs due to the extremely high conductivity of GNPs; GNP–TNT nanocomposite modified biosensor also exhibited lower charging current, smaller electrochemical interference from the surface functional groups and higher signal-noise ratio compared with GNPs modified biosensor. The curly and tubular titanate nanotubes (a few nanometers in diameter and a few hundred nanometers in length) are capable of providing a preferable biocompatible environment for the embedded HRP molecules than the bulky and tabulate graphene nanoplatelets (the thickness is between 4–20 nm and the diameter is about few micrometers). In summary, GNP–TNT nanocomposite has reached a balance between electrical conductivity and biocompatibility, which could account for the enhancement of HRP biosensor performance when being used as an electrode immobilization material.

Acknowledgment

This work was financially supported by the China Postdoctoral Science Foundation funded project (No. 2012M511569) and the Scientific Research Foundation for the Returned Overseas Chinese Scholars, State Education Ministry.

References

Feng, Q., Liu, K., Fu, J., Zhang, Y., Zheng, Z., Wang, C., Du, Y., Ye, W., 2012. Electrochimica Acta 60, 304–308.
Gao, Z.-D., Guan, F.-F., Li, C.-Y., Liu, H.-F., Song, Y.-Y., 2013. Biosensors and Bioelectronics 41, 771–775.
Iwabuchi, A., Choo, C.-K., Tanaka, K., 2004. Journal of Physical Chemistry B 108, 10863–10871.
Liu, X., Feng, H., Zhang, J., Zhao, R., Liu, X., Wong, D.K.Y., 2012. Biosensors and Bioelectronics 32, 188–194.
Neumann, B., Bogdanoff, P., Tributsch, H., Sakthivel, S., Kisch, H., 2005. Journal of Physical Chemistry B 109, 16579–16586.
Perera, S.D., Mariano, R.G., Vu, K., Nour, N., Seitz, O., Chabal, Y., Balkus, K.J., 2012. ACS Catalysis 2, 949–956.
Pizem, H., Sukenik, C.N., Sampathkumaran, U., McIlwain, A.K., De Guire, M.R., 2002. Chemistry of Materials 14, 2476–2485.
Shan, C., Yang, H., Song, J., Han, D., Ivaska, A., Niu, L., 2009. Analytical Chemistry 81, 2378–2382.
Shao, Y., Zhang, S., Wang, C., Nie, Z., Liu, J., Wang, Y., Lin, Y., 2010. Journal of Power Source 195, 4600–4605.
Tung, T.T., Kim, T.Y., Shim, J.P., Yang, W.S., Kim, H., Suh, K.S., 2011. Organic Electronics 12, 2215–2224.
Xiao, P., Zhang, Y., Cao, G., 2011. Sensors and Actuators B 155, 159–164.
Xu, Y.-J., Zhuang, Y., Fu, X., 2010. Journal of Physical Chemistry C 114, 2669–2676.
Zhang, H., Lv, X., Li, Y., Wang, Y., Li, J., 2009. ACS Nano 4, 380–386.
Zhang, M., Jin, Z., Zhang, J., Guo, X., Yang, J., Li, W., Wang, X., Zhang, Z., 2004. Journal of Molecular Catalysis A: Chemical 217, 203–210.
Zhang, Y., Tang, Z.-R., Fu, X., Xu, Y.-J., 2011. ACS Nano 5, 7426–7435.